Design of Waveguide Finline Arrays for Spatial Power Combining

Pengcheng Jia, *Student Member, IEEE*, Lee-Yin Chen, Nai-Shuo Cheng, *Member, IEEE*, and Robert A. York, *Senior Member, IEEE*

***Abstract*—Dense arrays of tapered-slot or finline transitions have proven useful in the design of compact spatial power combiners. In this paper, a design procedure is established for tapered finline arrays, providing a broad-band impedance match to a target load over the waveguide band. The procedure is based on an extension of the Klopfenstein optimal taper design to a non-TEM waveguiding structures, and employs the spectral-domain method to the computation of propagation constants in the array structure. The method has been experimentally verified for a small *X*-band array. Data is also presented, which shows that insertion loss in the finline arrays is independent of the number of array elements, assuming the designs are optimized for the desired return-loss characteristics in each case.**

***Index Terms*—Finline, spatial power-combining, waveguide.**

I. Introduction

SPATIAL or quasi-optical power-combining arrays have been successfully implemented in a "tray" architecture [1]–[3], as shown in Fig. 1. The tray approach permits the use of broad-band traveling-wave antennas and improved functionality through circuit integration along the direction of propagation. Each tray [see Fig. 1(a)] consists of a number of tapered-slotline or finline transitions, which coupled energy to and from a rectangular waveguide aperture to a set of monolithic-microwve integrated-circuit (MMIC) amplifiers. The finline transitions rest over a notched opening in the metal carrier to which the MMIC are attached. When the trays are stacked vertically, as shown in Fig. 1(b), the notched carriers form a rectangular waveguide aperture populated with the finline transitions. The use of the waveguide mode to distribute and collect energy to and from the set of amplifiers thus avoids loss mechanisms that limit the efficiency in corporate combiner structures.

The central problem in the design of the finline combiner systems is the electromagnetic design of the tapered-slot or finline transitions. The length and shape of the taper must be chosen to provide the desired impedance level at the MMICs over the desired bandwidth and, thus, determines the overall return loss of the structure. Standard field simulators have the ability to analyze the field in the fixed waveguide, but it does not have the function of synthesizing an unknown structure. This paper considers the design of the structure for a specified return-loss characteristic, using an extension of the theory or small reflections used to synthesize continuously tapered impedance transformers.

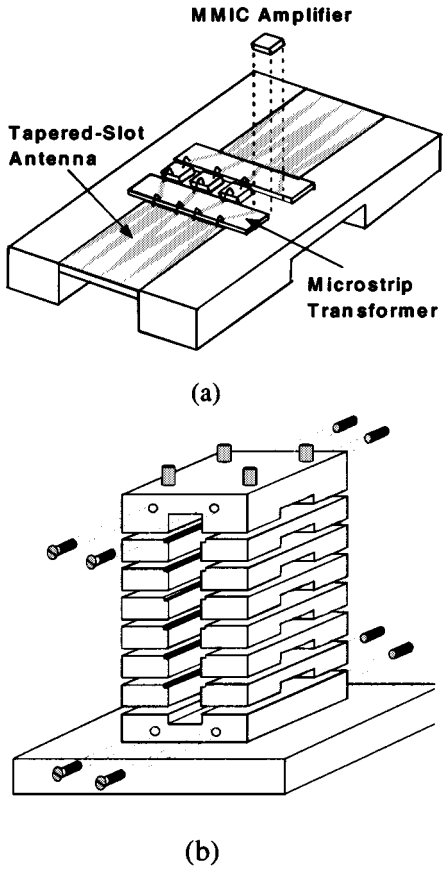

Fig. 1. Schematic illustration of the waveguide-based "tray" combiner. (a) Individual tray showing finline or tapered-slot transitions and MMICs, along with microstrip interconnects. (b) Assembled system with end caps, forming input and output waveguide apertures.

II. Synthesis of Tapered Finline Arrays

The design problem is illustrated in Fig. 2 and can be summarized as follows. Given the physical dimensions of the input and output gaps, along with the waveguide and substrate parameters, find the shape of the taper to realize a specified bandwidth and return loss. The problem is directly analogous to the

Manuscript received July 20, 2000, revised November 1, 2000. This work was supported in part by the Defense Advanced Research Projects Agency under the Microwave Analog Front End Technology Program through a subcontract from North Carolina State University under Contract DAAL01-96-K-3619 and in part by the Army Research Office Multidisciplinary Research Initiative Program under Grant DAAG55-98-1-0001.

P. Jia, L.-Y. Chen, and R. A. York are with the Electrical and Computer Engineering Department, University of California at Santa Barbara, Santa Barbara, CA 93106 USA.

N.-S. Cheng is with Conexant Systems Inc., Newbury Park, CA 91320 USA.

Publisher Item Identifier S 0018-9480(01)02427-9.

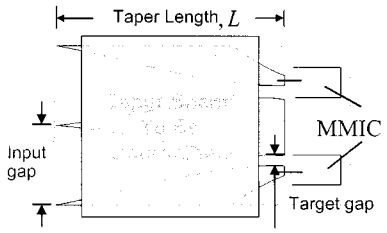

Fig. 2. Illustration of the problem statement, to determine the optimum taper shape in a multiple finline structure for matching to a set of MMICs.

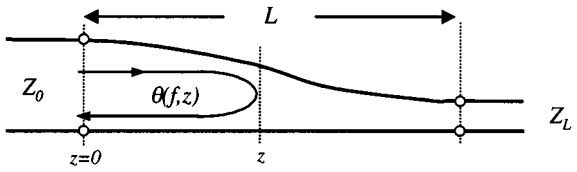

Fig. 3. Equivalent tapered transmission-line circuit for modeling the finline array.

synthesis of tapered transmission-line impedance transformers. From the theory of small reflections [4], it can be shown that gradual impedance taper on a non-TEM line has an input reflection coefficient

$$\Gamma_{\text{in}}(f) = \frac{1}{2}\int_0^{\theta_t} e^{-j\theta}\frac{d}{d\theta}\ln\left(\frac{Z(\theta)}{Z_0}\right)d\theta \tag{1}$$

where z is the position along the taper, L is the taper length, β is the propagation constant, Z_0 represents the reference impedance at the input end of the taper, and

$$\theta(f,z) = \int_0^z 2\beta(f,z')dz' \tag{2}$$

is the roundtrip phase delay to a point z along the taper, as shown in Fig. 3. The total roundtrip phase delay is $\theta_t = \theta(f,L)$.

The function $Z(\theta)$ describes the variation in impedance along the taper, and is an implicit function of z. In order to maintain an input reflection coefficient $\Gamma < \Gamma_m$ over the desired bandwidth, it has been shown [4], [5] that $Z(\theta)$ must take the form

$$\ln\frac{Z(\theta)}{Z_0} = \frac{1}{2}\ln\frac{Z_L}{Z_0} + \Gamma_m A^2 F\left(\frac{2\theta}{\theta_t} - 1, A\right) \tag{3}$$

where Z_L is the terminating impedance and

$$A = \cosh^{-1}\left(\frac{\Gamma_0}{\Gamma_m}\right)$$

$$\Gamma_0 = \frac{1}{2}\ln\left(\frac{Z_L}{Z_0}\right)$$

$$F(x,A) = -F(-x,A) = \int_0^x \frac{I_1(A\sqrt{1-y^2})}{A\sqrt{1-y^2}}dy$$

and $I_1(x)$ is the modified Bessel function of the first kind and first order. The passband is defined as $\theta_t > 2A$. Assuming the propagation constant is a monotonically increasing function of frequency, the lowest operating frequency is, therefore, defined by

$$\theta_t(f_0) = 2A \tag{4}$$

which is an implicit relationship between the taper length L, the lower cutoff frequency f_0, and the maximum reflection coefficient Γ_m.

The main difficulties in applying the above results are the frequency dependence of the wave impedance and propagation constant, and the difficulty in translating the impedance as a function of θ into a function of z, and subsequently determining the physical parameters required to synthesize the impedance taper. The frequency dependence of the wave impedance and propagation constant means that the result (3) will, in general, require a different physical taper at each frequency, which is obviously not possible to implement. However, for the finline transitions, the normalized impedance $Z(\theta)/Z_0$ is found to be a relatively weak function of frequency. We, therefore, design the taper at a fixed frequency, chosen to be f_0. In addition, it has been found that the waves propagating along the finline structures are approximately TE in character, which allows us to relate the wave impedance to propagation constant as

$$Z = \frac{\omega\mu}{\beta}. \tag{5}$$

Using wave impedances instead of characteristic impedance, (3) can now be rewritten in terms of β

$$\beta(f_0,z) = \sqrt{\beta_L\beta_0}\exp\left[-\Gamma_m A^2 F\left(\frac{2\theta(f_0,z)}{\theta_t} - 1, A\right)\right] \tag{6}$$

where β, β_L, and β_0 correspond to Z, Z_L, and Z_0, respectively, using (5). To compute the required propagation constant as a function of the position along the taper $\beta(z)$, the taper structure is divided into N sections of length $\Delta z = L/N$, and θ can be approximated by

$$\theta(z_i) \approx \sum_{k=0}^{i-1} 2\beta(z_k)\Delta z = \theta(z_{i-1}) + 2\beta(z_{i-1})\Delta z \tag{7}$$

where $z_i = i\Delta z$. Noting that $\theta(0) = 0$, we first evaluate $\beta(0)$ from (6), and then use the approximation (7) in (6) to evaluate all subsequent values of $\beta(z_i)$ along the taper. We then repeat the iterative process until the solution set of β converges. The resulting procedure is similar to that used in [6] for single finline structures. Note that the propagation constants at the ends of the taper do not match the target values $\beta(0) \neq \beta_0$ and $\beta(L) \neq \beta_L$. Using (6), it can be shown that

$$\beta(L) = \beta_L e^{\Gamma_m} \tag{8}$$

and this either fixes the maximum reflection coefficient for a given $\beta(L)$ or determines $\beta(L)$ for a given Γ_m. For a dense finline array, there is a potentially large impedance discontinuity in going from an unloaded waveguide to the loaded waveguide, thus, it is necessary to manipulate the substrate material, thickness, tray locations, and local waveguide width in order to satisfy (8) for a desired Γ_m. Another possibility is to include a quarter-wave "notch" transformer as part of the finline transition [7], but this was proven impossible in this study due to the use of ceramic substrates, which were difficult to machine.

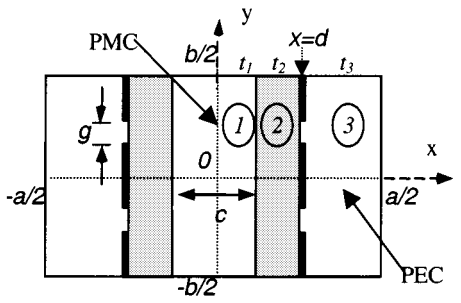

Fig. 4. Cross section of a 2 × 2 finline array in a standard waveguide environment.

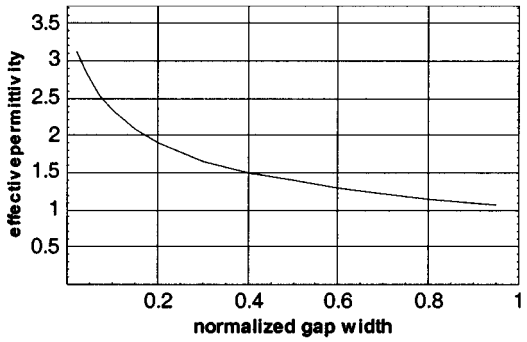

Fig. 5. Effective permittivity versus normalized gap width for a 2 × 2 finline arary in WR90 waveguide.

III. Propagation Constant of Finline Array

In this paper, the spectral-domain method (SDM) [8], [9] was used to find the relationship between the propagation constant and geometrical parameters of the finline—most importantly, the slot width. For simplicity, a 2 × 2 finline array was analyzed, as shown in Fig. 4. We assume perfect contact between the finline and waveguide walls. Symmetries along the major axes were used to reduce the computation domain to the upper right quadrant of Fig. 4.

In the SDM, the electric fields and currents in each region are expanded as a Fourier series in y. Denoting the electric field in the ith region as E_i

$$\begin{aligned} E_i &= \sum_{n=-\infty}^{\infty} \tilde{E}_i e^{j\alpha_n y}, \qquad \text{where } \alpha_n = \frac{2n\pi}{b} \\ \tilde{E}_i &= \frac{2}{b}\int_0^{b/2} E_i e^{j\alpha_n y} dy. \end{aligned} \tag{9}$$

Applying the boundary conditions at the interface $x = d$ gives the following two algebraic equations:

$$\begin{aligned} Y_{yy}\tilde{E}_y + Y_{yz}\tilde{E}_z &= j\omega\mu_0 \tilde{J}_y \\ Y_{zy}\tilde{E}_y + Y_{zz}\tilde{E}_z &= j\omega\mu_0 \tilde{J}_z \end{aligned} \tag{10}$$

where $\tilde{J}$ are the unknown currents on the fins. Using the equivalent transmission-line "immitance" concept [9], we find

$$\begin{aligned} Y_{yy} &= j\omega\mu_0\left(Y_{\mathrm{TE}}\cos^2\theta + Y_{\mathrm{TM}}\sin^2\theta\right) \\ Y_{yz} &= -Y_{zy} = -\omega\mu_0 \sin\theta\cos\theta(Y_{\mathrm{TM}} - Y_{\mathrm{TE}}) \\ Y_{zz} &= j\omega\mu_0\left[Y_{\mathrm{TE}}\sin^2\theta + Y_{\mathrm{TM}}\cos^2\theta\right] \end{aligned} \tag{11}$$

where

$$\begin{aligned} \sin\theta &= \frac{\beta}{\sqrt{\beta^2+\alpha_n^2}} \\ \cos\theta &= \frac{\alpha_n}{\sqrt{\beta^2+\alpha_n^2}} \\ \Gamma_{ni} &= \sqrt{\beta^2+\alpha_n^2-\omega^2\mu_0\varepsilon_i} \\ Y_{\mathrm{TM}i} &= \frac{j\omega\varepsilon_i}{\Gamma_{ni}} \\ Y_{\mathrm{TE}i} &= \frac{\Gamma_{ni}}{j\omega\mu_0} \\ Y_{\mathrm{TM}L} &= Y_{\mathrm{TM}1}\tanh(\Gamma_{n1}t_1) \\ Y_{\mathrm{TE}L} &= Y_{\mathrm{TE}1}\tanh(\Gamma_{n1}t_1) \end{aligned}$$

$$\begin{aligned} Y_{\mathrm{TM}} &= Y_{\mathrm{TM}2}\frac{Y_{\mathrm{TM}L} + Y_{\mathrm{TM}2}\tanh(\Gamma_{n2}t_2)}{Y_{\mathrm{TM}2} + Y_{\mathrm{TM}L}\tanh(\Gamma_{n2}t_2)} \\ &\quad + Y_{\mathrm{TM}3}\coth(\Gamma_{n3}t_3) \\ Y_{\mathrm{TE}} &= Y_{\mathrm{TE}2}\frac{Y_{\mathrm{TE}L} + Y_{\mathrm{TE}2}\tanh(\Gamma_{n2}t_2)}{Y_{\mathrm{TE}2} + Y_{\mathrm{TE}L}\tanh(\Gamma_{n2}t_2)} \\ &\quad + Y_{\mathrm{TE}3}\coth(\Gamma_{n3}t_3). \end{aligned}$$

The unknown aperture fields E_y and E_z are expanded in terms of a basis set of rectangular pulses ξ_i and η_i, which is better for the wide slot portion in the finline, and then Fourier transformed to

$$\begin{aligned} \tilde{E}_y(\alpha_n) &= \sum_{i=1}^{N_y} c_i\tilde{\xi}_i(\alpha_n) \\ \tilde{E}_z(\alpha_n) &= \sum_{i=1}^{N_z} d_i\tilde{\eta}_i(\alpha_n). \end{aligned} \tag{12}$$

Substituting (12) into (10) and integrating gives the homogeneous matrix equation

$$\begin{aligned} \sum_{i=1}^{N_y} K_{pi}^{yy}(\beta)c_i + \sum_{j=1}^{N_z} K_{pj}^{yz}(\beta)d_j &= 0, \qquad p = 1,\ldots,N_y \\ \sum_{i=1}^{N_y} K_{qi}^{zy}(\beta)c_i + \sum_{j=1}^{N_z} K_{qj}^{zz}(\beta)d_j &= 0, \qquad q = 1,\ldots,N_z. \end{aligned} \tag{13}$$

The propagation constants over the normalized gap $2g/b$ are then found from the characteristic equation obtained by setting the determinant of the coefficient matrix in (13) to zero. Fig. 5 shows the results of this calculation for a representative physical situation of interest, corresponding to two 10-mil-thick aluminum nitride (AlN) substrates, with a separation of $c = 5$ mm, placed in an X-band (WR-90) waveguide with dimension $a = 0.9''$, $b = 0.4''$. A single "pulse" basis function was used in this calculation.

The waveguide aperture and number of transitions per tray determine the input gap size, but we have not yet addressed the choice of a target gap size. The target gap is determined by the desired impedance level for the MMIC amplifier. For most off-the-shelf MMICs, this gap should be chosen for a 50-Ω impedance. Unfortunately, this is not possible in general for slotline on commonly used substrate materials. Our approach

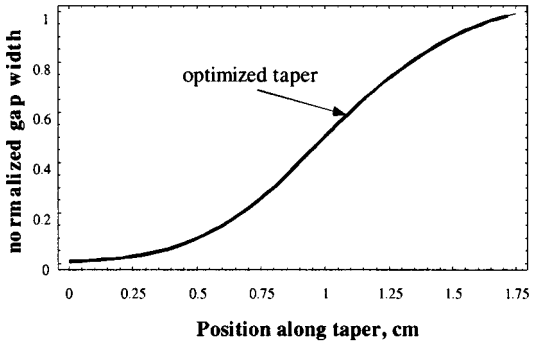

Fig. 6. Normalized gap width versus location along the optimal tapered finline.

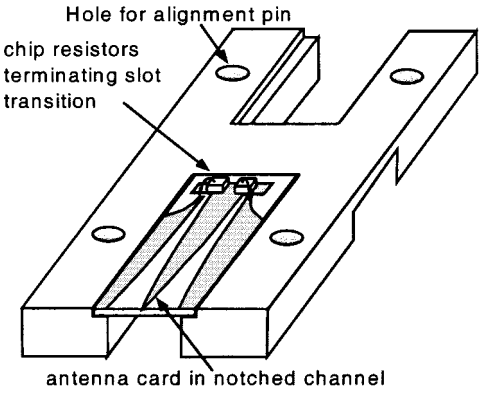

Fig. 7. Finline transitions terminated in resistive loads for design verification.

was, therefore, to choose the smallest realizable gap dimension, giving some impedance that is larger than 50 Ω, and include a final impedance transformation to the MMIC in microstrip as part of the slot-line-to-microstrip transition.

IV. Optimized Taper and Experimental Verification

Using the results in Fig. 5 in the design procedure summarized in Section III, an "optimized" taper was computed for an input reflection coefficient of −20 dB. This is shown in Fig. 6.

The taper design was tested experimentally by terminating the slots in a resistive matched load, using 100-Ω chip resistors, as depicted in Fig. 7. Two trays were then stacked and placed centrally in a WR90 waveguide, and return-loss measurements were made. The measured return loss is shown in Fig. 8, along with the theoretical predictions using the theory of Sections III and IV. A good impedance match is observed over the measured bandwidth, which was limited to 8.2–12.4 GHz due to the calibration standards used. Discrepancies between the two curves are attributed to some additional series inductance from the bonding of the chip resistors.

V. Scaling, Losses, and Combining Efficiency

The design in Fig. 6 was used as the basis of several GaAs combiners. Since the design procedure was somewhat laborious, the taper design based on a 2 × 2 array was scaled to larger arrays. In the combiner reported in [3], two additional trays were added to form a 2 × 4 array. Fig. 9 shows the measured reflection coefficient for various terminating resistances. Not surprisingly,

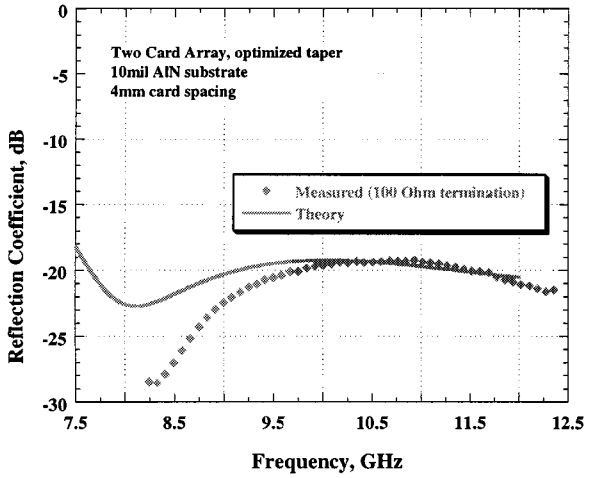

Fig. 8. Comparison of measured reflection coefficient with theoretical predictions for a 2 × 2 finline array in WR90 waveguide, using the taper design of Fig. 6.

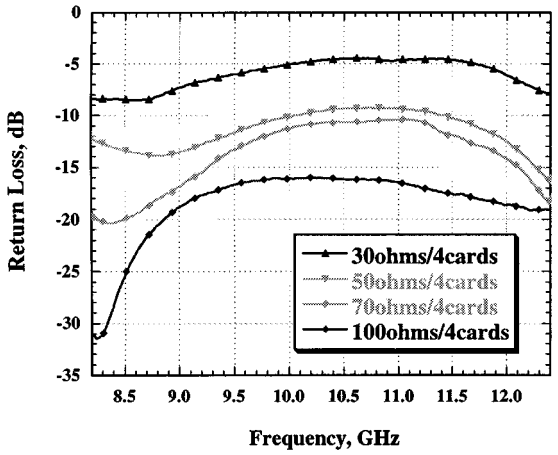

Fig. 9. Measurements for a four-tray system for various terminating resistances.

some degradation in return loss is observed for 100-Ω resistors, as compared with the two-tray result of Fig. 8; nevertheless, better than 15-dB return loss is maintained over the band, and this proven satisfactory for the active combiner system.

The 2 × 2 tray was then scaled to a 4 × 6 design. In this case, the number of finline transitions on each tray was doubled to four by linearly scaling the dimensions of the 2 × 2 design. The number of trays was increased to six, which required the use of a thinner tray and, hence, closer tray-to-tray spacing. In this case, two-port measurements were performed in order to examine the return- and insertion-loss characteristics of the passive structure. The layout of the test circuit (Fig. 10) consists of back-to-back finline transitions with 50-Ω microstrip lines used in place of active elements. As a consequence of the reduced tray spacing, the terminating resistance yielding the best impedance match was lowered to 70 Ω, thus, a 70–50-Ω taper was included in the microstrip through line.

Measured S_{11} and S_{21} for two-tray (4 × 2) and six-tray (4 × 6) system are shown in Fig. 11. Note that the two-tray result is quite good and consistent with the results observed in

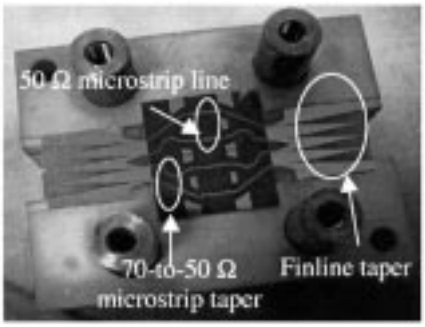

Fig. 10. Tray layout for a through measurement.

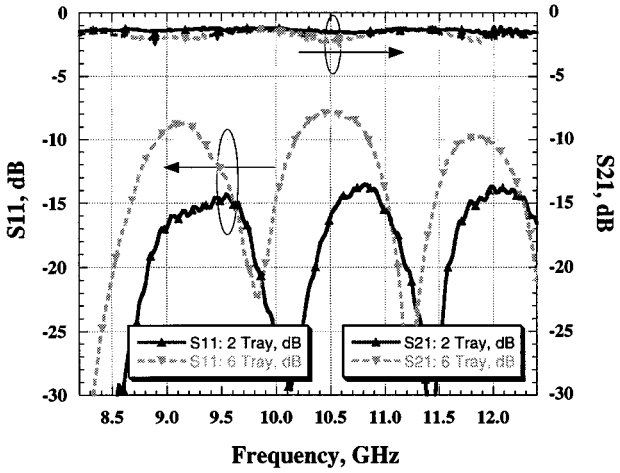

Fig. 11. Two-port measurements for the finline arrays.

Fig. 9. The six-tray system (24 transitions) suffers significantly increased reflection losses. Since the separation between the trays in the 4 × 6 system is the same as the 4 × 2 system, the deterioration comes from the nonoptimized taper, not the intertray coupling. Nevertheless, an important observation can be made with respect to insertion loss. Ignoring the effects of reflection losses (which can potentially be recovered by properly optimizing the finline taper for the 4 × 6 array), the insertion losses appear approximately constant in the two- and six-tray system. This is a natural result of the parallel nature of the transitions, but has important consequences in combining efficiency when scaling the combiners to large numbers of devices. Whereas corporate combiners suffer a reduction in combining efficiency as the number of devices is increased, the spatial combiners exhibit a loss that is roughly independent of the number of devices.

To empirically quantify this assertion using the measured results of Fig. 11, we compute a "dissipative loss" as

$$\text{Loss} = \frac{P_{\text{load}}}{P_{\text{forward}}} = \frac{P_{\text{load}}}{P_{\text{in}} - P_{\text{reflection}}} = \frac{|S_{21}|^2}{1 - |S_{11}|^2}. \quad (14)$$

The losses computed from (14) for a two-, six-, and eight-tray configuration are plotted in Fig. 12, showing that the dissipative loss in each case is approximately constant and independent of the number of trays.

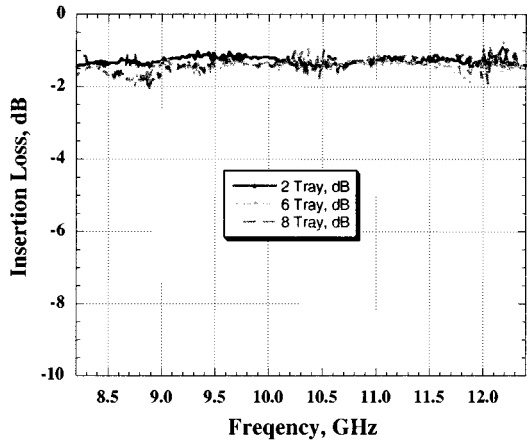

Fig. 12. Measured dissipative loss for two-, six-, and eight-tray finline array with though lines.

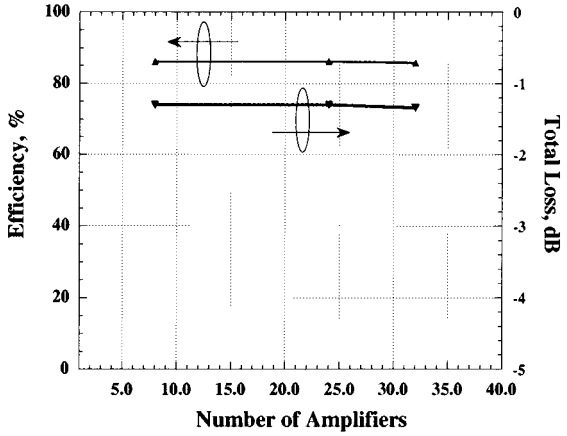

Fig. 13. Efficiency and total insertion loss of power combiner versus number of elements in finline array.

It can then be shown that the maximum combining efficiency η_c of a spatial combiner structure is

$$\eta_c \approx L_o \quad (15)$$

where L_o is the loss associated with the combiner circuit (post-amplification losses). In the present case, any loss can be attributed equally to the input and output antennas, which gives us an estimate of the maximum potential combining efficiency as

$$\eta_c \approx \sqrt{\frac{|S_{21}|^2}{1 - |S_{11}|^2}}. \quad (16)$$

Loss and efficiency based on (14) and (16) is shown in Fig. 13, using an average loss over the band from the measured two-port results of Fig. 11 and similar measurements for an eight-tray system.

The structure can be scaled up to accommodate more devices. Fig. 13 shows a very small reduction in combining efficiency when the elements increase from 8 to 32. The maximum number of elements will be determined by both the separation between trays and size of the waveguide.

As to the failure in a spatial power-combiner system, the impact of failed elements on the total loss is analyzed in [12]. The array will degrade gracefully, in agreement with the theoretical analysis.

VI. Conclusion

A design procedure for dense finline arrays has been developed and applied to the design of active combiner systems. The design example used in this paper formed the basis of successful combiner implementations reported in [3] and [10]. This paper has explored the limits of scaling tapered finline structures to increasingly dense configurations, showing that the degradation in return loss is graceful, but can become significant when designs are scaled by large multipliers. We have also shown that the dissipative loss in such finline arrays is approximately independent of the number of transitions used, which provides a compelling argument for the use of spatial combiner systems for combining the power from large numbers of active devices. Future work includes using more sophisticated optimization procedures [11] to improve the design of the arrays.

References

[1] N.-S. Cheng, "Waveguide-based spatial power combiners," Ph.D. dissertation, Dept. Elect. Comput. Eng., Univ. California at Santa Barbara, Santa Barbara, CA, 1999.

[2] A. Alexanian and R. A. York, "Broad-band spatially combined amplifier array using tapered slot transitions in waveguide," *IEEE Microwave Guided Wave Lett.*, vol. 7, pp. 42–44, Feb. 1997.

[3] N.-S. Cheng, A. Alexanian, M. G. Case, D. B. Rensch, and R. A. York, "40-W CW broad-band spatial power combiner using dense finline arrays," *IEEE Trans. Microwave Theory Tech.*, vol. 47, July 1999.

[4] D. M. Pozar, *Microwave Engineering*, 2nd ed. New York: Wiley, 1998.

[5] R. W. Klopfenstein, "A transmission-line taper of improved design," *Proc. IRE*, vol. 442, pp. 31–35, Jan. 1956.

[6] Schieblich, J. K. Piotrowski, and J. H. Hinken, "Synthesis of optimum finline tapers using dispersion formulas for arbitrary slot widths and locations," *IEEE Trans. Microwave Theory Tech.*, vol. MTT-32, pp. 1638–1644, Dec. 1984.

[7] C. Verver and W. Hoefer, "Quarter-wave matching of waveguide-to-finline transitions," *IEEE Trans. Microwave Theory Tech.*, vol. MTT-32, pp. 1645–1648, Dec. 1984.

[8] L. P. Schmidt and T. Itoh, "Spectral domain analysis of dominant and higher order modes in fin-lines," *IEEE Trans. Microwave Theory Tech.*, vol. MTT-28, pp. 981–985, Sept. 1980.

[9] T. Itoh, "Spectral domain immitance approach for dispersion characteristics of generalized printed transmission lines," *IEEE Trans. Microwave Theory Tech.*, vol. MTT-28, pp. 733–737, July 1980.

[10] N.-S. Cheng, P. Jia, D. B. Rensch, and R. A. York, "A 120-W X-band spatially combined solid-state amplifier," *IEEE Trans. Microwave Theory Tech.*, vol. 48, pp. 2557–2561, Dec. 1999.

[11] C. A. W. Vale and P. Meyer, "Designing high-performance finline tapers with vector-based optimization," *IEEE Trans. Microwave Theory Tech.*, vol. 47, pp. 2467–2472, Dec. 1999.

[12] D. B. Rutledge, N.-S. Cheng, R. A. York, R. M. Weikle, and M. P. De Lisio, "Failure in power-combining arrays," *IEEE Trans. Microwave Theory Tech.*, vol. 47, pp. 1077–1082, July 1999.

Pengcheng Jia (S'98) received the B.S. degree in electronics science and information system from Nankai University, Tianjin, China, in 1995, the M.S. degree in electrical engineering from Tsinghua University, Beijing, China, in 1998, and is currently working toward the Ph.D. degree in electrical and computer engineering at the University of California at Santa Barbara.

His current research involves the development of waveguide-based broad-band high-power spatial power combiners and power amplifiers using GaN devices.

Lee-Yin Chen received the B.S. degree in electrical engineering from the National Taiwan University, Taipei, Taiwan, R.O.C., in 1997, the M.S. degree in electrical engineering from the University of California at Santa Barbara (UCSB), in 1999, and is currently working toward the Ph.D. degree at the UCSB.

Her current research involves the development of waveguide-based spatial power combining in microwave frequency and high-frequency power-amplifier design.

Nai-Shuo Cheng (S'96–M'99) received the B.S. degree in nuclear engineering from the National Tsing Hua University, Hsinchu, Taiwan, R.O.C., in 1989, the M.S.E.E. degree in electrical engineering from Syracuse University, Syracuse, NY, in 1994, and the Ph.D. degree in electrical and computer engineering from the University of California at Santa Barbara, in 1999

He is currently with Conexant Systems Inc., Newbury Park, CA. His research involves the development of waveguide-based spatial power-combiner circuits and the study of the propagation characteristics for non-TEM waveguiding structures by using the finite-difference method.

Dr. Cheng was the second-place recipient of the 1998 Student Paper Competition at the IEEE Microwave Theory and Techniques Society (IEEE MTT-S) International Microwave Symposium.

Robert A. York (S'85–M'89–SM'99) received the B.S. degree in electrical engineering from the University of New Hampshire, Durham, in 1987, and the M.S. and Ph.D. degrees in electrical engineering from Cornell University, Ithaca, NY, in 1989 and 1991, respectively.

He is currently an Associate Professor of electrical and computer engineering at the University of California at Santa Barbara (UCSB), where his group is currently involved with the design and fabrication of novel microwave and millimeter-wave circuits, microwave photonics, high-power microwave and millimeter-wave modules using spatial combining and wide-bandgap semiconductor devices, and application of ferroelectric materials to microwave and millimeter-wave circuits and systems.

Dr. York was the recipient of the 1993 Army Research Office Young Investigator Award and the 1996 Office of Naval Research Young Investigator Award.